

Autonomous Sea Turtle Robot for Marine Fieldwork

Zach J. Patterson^{1,2*†}, Emily Sologuren^{2†}, Levi Cai^{2,3},
Daniel Kim², Alaa Maalouf^{4, 2}, Pascal Spino², Daniela Rus^{2*}

^{1*}Mechanical and Aerospace Engineering, Case Western Reserve University, Cleveland, 44106, USA.

²Computer Science and Artificial Intelligence Laboratory, Massachusetts Institute of Technology, Cambridge, 02139, USA.

³Applied Ocean Physics and Engineering Department, Woods Hole Oceanographic Institution, Woods Hole, 02543, USA.

⁴Computer Science, University of Haifa, Haifa, 3498838, Israel.

*Corresponding author(s). E-mail(s): zpatt@case.edu; rus@csail.mit.edu;
Contributing authors: esolo@mit.edu; cail@mit.edu; dkim6@exeter.edu;
alaamaalouf@cs.haifa.ac.il; spino@mit.edu;

†These authors contributed equally to this work.

Abstract

Autonomous robots can transform how we observe marine ecosystems [1–3], but close-range operation in reefs and other cluttered habitats remains difficult [4, 5]. Vehicles must maneuver safely near animals and fragile structures while coping with currents, variable illumination and limited sensing. Previous approaches simplify these problems by leveraging soft materials [6] and bioinspired swimming designs [7], but such platforms remain limited in terms of deployable autonomy [8–10]. Here we present a sea turtle-inspired autonomous underwater robot that closed the gap between bioinspired locomotion and field-ready autonomy through a tightly integrated, vision-driven control stack. The robot combines robust depth-heading stabilization with obstacle avoidance and target-centric control, enabling it to track and interact with moving objects in complex terrain. We validate the robot in controlled pool experiments and in a live coral reef exhibit at the New England Aquarium, demonstrating stable operation and reliable tracking of fast-moving marine animals and human divers. To the best of our knowledge, this is the first integrated biomimetic robotic system, combining novel hardware, control, and field experiments, deployed to track and

monitor real marine animals in their natural environment [11]. During off-tether experiments, we demonstrate safe navigation around obstacles (91% success rate in the aquarium exhibit) and introduce a low-compute onboard tracking mode. Together, these results establish a practical route toward soft-rigid hybrid, bioinspired underwater robots capable of minimally disruptive exploration [12] and close-range monitoring in sensitive ecosystems [13, 14].

Keywords: Bioinspired robotics, autonomy, deployability

Main Text:

1 Introduction

The ocean remains one of the least explored frontiers on Earth [15, 16], yet it plays a central role in regulating our planet’s climate, biodiversity, and life systems [17, 18]. To study and protect these vast and fragile ecosystems, we need machines that can move with the grace, efficiency, and resilience of marine life itself. Biomimetic robots, inspired by the form and function of aquatic organisms, offer a path forward [19–22]. By translating nature’s evolved designs into engineering, these autonomous systems promise a combination of maneuverability, efficiency, and environmental compatibility [23, 24]. Unlike traditional underwater robots that rely on thrusters for propulsion [25–27], biomimetic robots use nature-inspired swimming control to generate movement through coordinated oscillatory motions of flexible hydrofoils [28, 29]. This approach improves efficiency while maintaining agility, making such robots safer to deploy in sensitive habitats such as coral reefs. Biomimetic robots also hold strong potential to be less disruptive to marine wildlife [8, 12, 30, 31], positioning them as tools for scientific observation, exploration, and conservation.

While previous bioinspired aquatic robots have demonstrated impressive capabilities such as deep sea survivability [10], adaptive shape morphing [9], and rapid swimming speeds [32, 33], the real-world deployment of *autonomous* biomimetic robots remains limited. Most current platforms are engineered primarily for laboratory studies [34]. Adapting them for use in marine habitats poses substantial challenges: ruggedizing systems for saltwater exposure, unpredictable currents, and variable lighting conditions is significantly more demanding than operation in controlled freshwater pool settings [6]. Many existing designs remain teleoperated proofs of concept, lacking the integrated sensors and the control algorithms required for autonomous field research [8, 9, 35]. The autonomy of biomimetic marine robots, their ability to perceive, decide, and act independently, remains minimal limiting their operational utility [36, 37].

2 Robot Design

To address these gaps, we developed Crush, a sea turtle-inspired autonomous underwater robot designed for agile intelligent operation in complex environments (Fig. 1). The design philosophy for the robot aims to strike a balance between explicit biomimicry

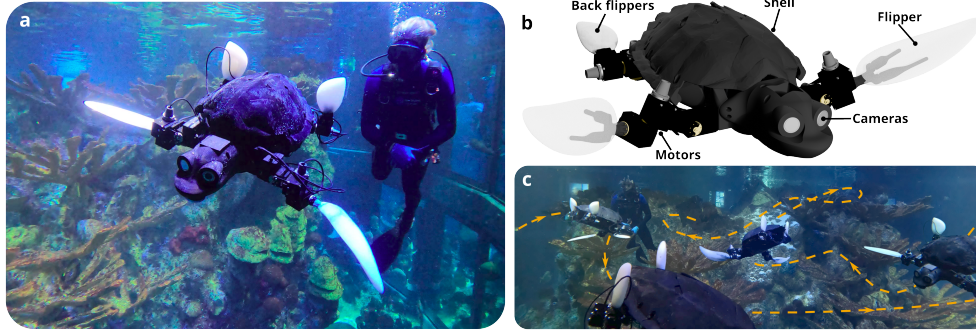


Fig. 1 Sea turtle-inspired robot for autonomous marine observation. **a**, A photograph of the turtle robot swimming in the New England Aquarium in Boston, MA. **b**, The turtle robot uses biomimetic soft-rigid flippers and visual feedback for tracking sea animals autonomously. **c**, Superimposed frames of robot swimming autonomously and untethered around coral in aquarium tank (the orange line denotes the path of the robot).

and pragmatic engineering necessity. There are several critical system components. First, the physical structure of the robot aims to mimic the morphology of a juvenile hawksbill sea turtle (*Eretmochelys imbricata*) [38]. The flippers are based on a simplified, idealized version of the skeletal and soft tissue structure of sea turtle flippers [28]. The skeletal components are 3D printed and overmolded into a silicone rubber matrix. The large front flippers are the main source of propulsion, while the smaller rear flippers serve as rudders. The front flippers are driven by three servomotors at each shoulder, allowing roll-pitch-yaw kinematics of the flippers that are necessary for approximating sea turtle underwater flight [39]. The rear limbs have two degrees of freedom each, pitch and yaw. The body of the sea turtle is printed out of rigid ABS plastic around a sealed acrylic tube hull, and the shell is directly adapted from 3D scans of a hawksbill turtle [40].

The robot contains two forward-facing cameras for vision, a small downward-facing sonar module, a depth sensor, and a nine axis inertial measurement unit (IMU). Together, these sensors enable the autonomous behaviors described below. Finally, the robot has a detachable tether for remote monitoring, teleoperation, and utilization of off-board compute resources. A high-level system diagram is shown in Fig. S1.

Crush combines several autonomous capabilities that enable collision-free swimming in cluttered environments, stable tracking of commanded headings and depths, and visual tracking of marine animals, objects, and other robots. It can run fully untethered or be operated with a tether for real-time data streaming and high-level supervision, giving field teams flexibility across experimental and deployment scenarios. As a result, Crush achieves a substantially higher level of autonomous functionality than prior turtle-inspired robotic platforms [9, 33].

We experimentally demonstrate autonomous behaviors that allow the robot to function in complex marine environments, including multi-gait swimming along arbitrary 3D trajectories, collision-free obstacle avoidance, and visual animal following.

These capabilities arise from a tightly integrated perception–control pipeline that fuses trajectory tracking with real-time visual sensing and closed-loop control.

A key element of the autonomy stack is a visual tracking pipeline that supports real-time following of arbitrary objects and animals. Targets are initialized on the latest frame by supplying point prompts to the Segment Anything Model (SAM) [41] to obtain a binary mask, and then track this mask across subsequent frames using the CUTIE tracker [42]. A lightweight health monitor detects drift and enables quick, non-disruptive re-initialization (e.g., via a simple gesture or click-based retargeting). Full details are provided in Methods Section 4.3.

The tracker output, namely the position of the centroid of the object, is mapped directly to the robot’s control input, which modulates the executed gait. All gaits are defined as variations of a baseline swimming pattern through a control vector $\mathbf{u} = [u_{\text{freq}}, u_{\text{roll}}, u_{\text{pitch}}, u_{\text{yaw}}]^T$, where the first (scalar) input controls the frequency of the gait and the other inputs modify the gait to produce net torques in the roll, pitch, and yaw directions, respectively. This parameterization allows for agile 3D locomotion. To operationalize this control input for tracking, the control inputs u_{pitch} and u_{yaw} are modified proportionally to the position of the tracked object with respect to the center of the frame, resulting in visual servoing. If the track is lost, the robot executes a recovery behavior by continuing to move in the direction implied by the object’s last observed position. Despite its simplicity, this policy effectively recovers in many common scenarios, particularly when the object exits the observation frame laterally. It is less effective when the animal swims rapidly above or below the robot, where vertical maneuverability and acceleration become limiting factors.

3 Results

We conducted experiments in the MIT Alumni Pool and the Giant Ocean Tank (GOT) at the New England Aquarium (NEA) in Boston, MA. The tank is 40 feet wide, 23 feet deep, and holds 200,000 gallons of saltwater. Our tracking experiments involved following various sea animals within the NEA Aquarium. The robot ends a track either when the targeted sea animal stops swimming or when an arbitrary depth limit is surpassed. For example, to maintain visibility of the robot from the observation deck, we stop a track if the target sea animal swims deeper than 7 meters. Successful tracks include several individual sea turtles, barracudas, stingrays, and divers. The longest track was of a 550 pound Green Sea Turtle (*Chelonia mydas*) named Myrtle (see Fig. 2). Crush follows Myrtle from one end of the tank to the other, until the sea turtle decides to stop. We conducted a total of 20 sea animal tracks, with a mean track time of 25.85 seconds and a standard deviation of 14.7 seconds. Of those 20 tracks, 12 were for sea turtles, 6 were for stingrays, and the last 2 were for barracudas. While the tracker was highly robust during experiments, there were, however, instances of the tracker failing. This occurred three times due specular/mirror-induced duplicates (appearance duplication), low-light/low-contrast regimes, stitching line distortions. We also validated our tracking pipeline at the MIT Alumni Pool, where we have 45 minutes of the robot tracking several inanimate objects, as well as a swimmer. We elaborate on the tracker’s failure modes and pool tests further in Methods Section 4.3.

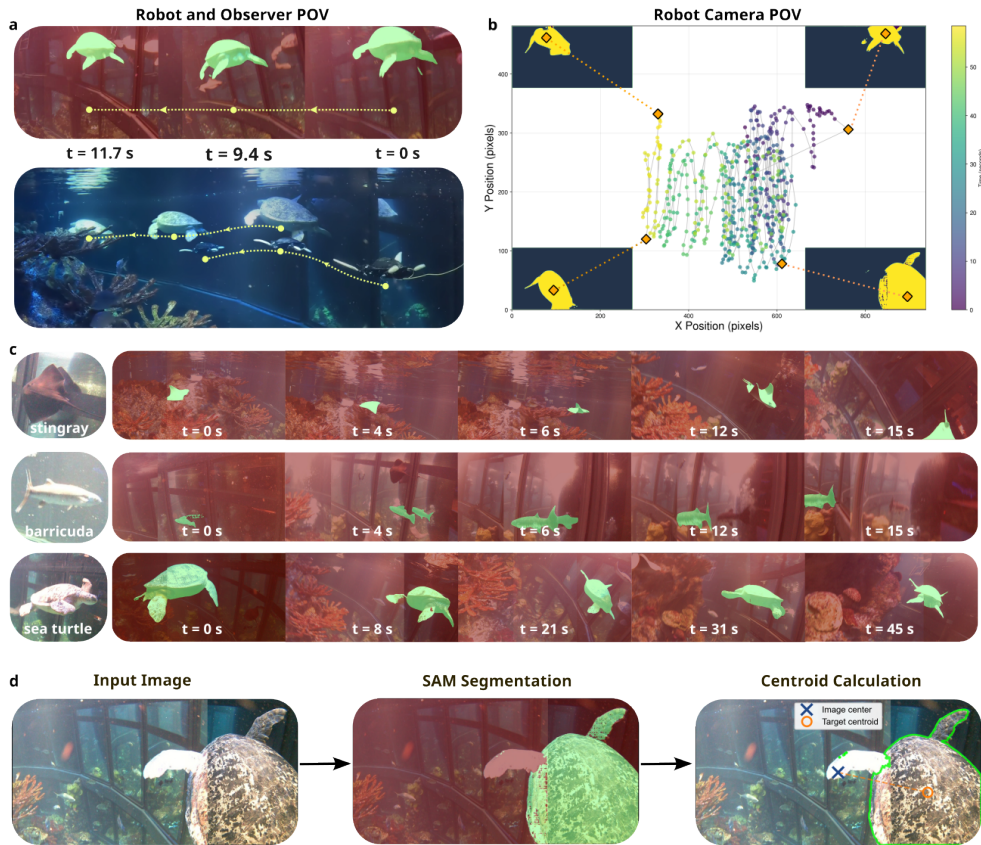


Fig. 2 Autonomous animal following. **a**, Time series showing the robot’s point of view (POV) with target segmentation masks (green overlays) during autonomous sea turtle tracking over ~ 12 seconds. **b**, Target centroid trajectories throughout a minute-long tracking sequence, with corner indices marking trajectory extremities (top left, top right, bottom left, and bottom right). **c**, Additional tracking examples: stingray track ending when the animal dived beneath the robot, barracuda track maintaining target lock despite specular reflections, and sustained sea turtle pursuit. **d**, Tracking pipeline: stereo cameras are stitched into a wide-field view, segmented to extract target centroid, which drives autonomous swimming control.

The robot is designed for fully untethered operation, with all perception and control running onboard. For some experiments, we attach a lightweight, detachable tether to enable real-time monitoring, limited teleoperation, and high-bandwidth data collection. We also conduct fully untethered trials, where the robot operates solely on its onboard sensing and autonomy stack, without external feedback or intervention.

In these autonomous deployments, the primary requirement is safe navigation in cluttered environments with reefs, animals, and walls. To achieve this, the robot turtle uses its forward-facing cameras to construct a stereo depth map of the scene. Although imperfect synchronization between the cameras introduces noise, simple filtering yields obstacle detections that are sufficiently reliable for control. When an

Table 1 Analyses of several aquarium tracks

Animal Type	Track duration (secs)	Failed	End Track Reason
Turtle	59	No	stopped swimming ^a
Turtle	57	No	stopped swimming ^a
Turtle	43	No	visibility
Turtle	38	No	coral collision ^b
Stingray	32	No	swam over robot
Stingray	30	No	too fast
Stingray	14	Yes	tracker failure
Barricuda	20	No	depth limitation
Barricuda	15	Yes	tracker failure

Several aquatic animals were observed and tracked in the Giant Ocean tank.
Full table available in Table S1

^a some tracks end early for the safety of the aquarium animals

^b track was not lost but ended early to prevent damage to robot

obstacle is detected closer than a predefined distance, the controller commands a strong yaw away from the centroid of the largest detected object, combined with a substantial roll. The resulting agile banking maneuver produces tight turns that effectively prevent collisions.

For untethered autonomy trials, we initialize the robot with a target depth and a nominal heading toward coral structures near the center of the tank, then allow it to operate independently for extended periods. Each time an obstacle is encountered, the desired heading is updated, leading to a random-walk-like exploratory trajectory around the exhibit. During these runs, there is no human intervention in guidance or control; only Aquarium divers are present to passively monitor the safety of the exhibit and animals.

We conducted three trials in the Aquarium of durations 132, 94, and 341 seconds (mean: 189 s, standard deviation 133 s). The number of avoidance events occurring during each experiment are 10, 7, and 28 respectively. The robot successfully avoided a variety of objects, including coral, divers, and the tank walls. An example of the robot avoiding the coral can be seen in Fig. 3. The robot successfully avoided 41 of 45 total detected obstacles autonomously (91.1% success rate). More importantly, only one of the four failed maneuvers involved a coral structure; the remaining three failures occurred on the walls of the glass tank, an artifact of the aquarium testing environment not present in natural reef deployments. One additional intervention occurred due to environmental entanglement that was unrelated to the robot’s navigation performance. An alternative metric is seconds per intervention (similar to the industry standard “miles per intervention” metric for self-driving vehicles), which is 113.5 seconds for this data. We further evaluated autonomous obstacle avoidance experiments in the MIT Alumni pool, through three trials totaling 20.2 minutes. The robot executed a total of 162 avoidance maneuvers in response to several physical objects (walls, pool stairs, floating objects) with a 95.4% success rate, which is discussed more in Methods Section 4.4.

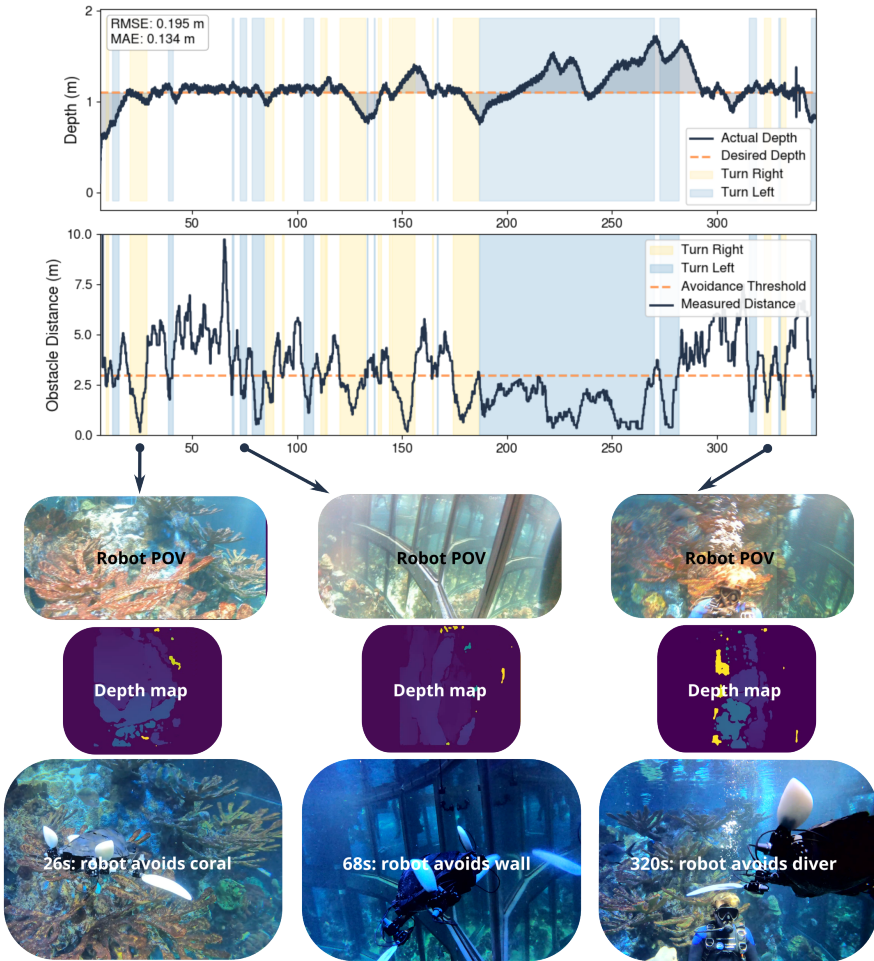


Fig. 3 Autonomous underwater obstacle avoidance. **Top**, Depth over time showing the robot maintaining a target depth of 1.1 m (RMSE = 0.195 m, MAE = 0.134 m). **Bottom**, Obstacle distance estimates over time with the 2.5 m avoidance threshold (dashed); yellow and blue shaded regions indicate right and left turn commands, respectively. Annotated time points highlight three representative avoidance events—coral reef (26 s), glass wall (68 s), and a diver (320 s)—each shown with the robot’s stereo camera view (Robot POV), the corresponding stereo depth map, and an external observer perspective.

Finally, we validated that this tracking approach can be deployed onboard in fully untethered mode. We implemented and trained FOMO (Faster Objects, More Objects), a lightweight object-detection model optimized for real-time inference on the robot’s Raspberry Pi 5 computer. Tracking performance was evaluated in six controlled trials in which a static target was placed at three discrete lateral positions—leftmost, center, and rightmost within the tank—to assess detection consistency across the robot’s visual field. Fig. S4 shows a 34-second segment from a 234-second autonomous

tracking sequence at the MIT Alumni Pool; several additional experiments demonstrate the robot’s robust tracking capabilities. A more detailed analysis is provided in SI Section S3. The controlled pool environment supported robust long-duration tracks supported by a control strategy for recovery from mis-detections.

Taken together, these complementary experiments conducted in several environments show that embedded tracking can support extended autonomous operation under controlled conditions, while real-world deployments with unpredictable marine wildlife currently benefit from the higher reliability and throughput of more capable offboard hardware. Future work will focus on improving onboard robustness through model optimization and the integration of more powerful edge-compute devices.

To our knowledge, these are the first demonstrations of a biomimetic robot used to track and monitor real marine animals [11]. By leveraging effective continuous gait modification in various vision-related autonomy strategies, this pipeline for biomimetic robot autonomy is interpretable and effective, allowing human-in-the-loop scientific observation or safe fully autonomous deployment. Despite the simplicity of many of our underlying methods, the resulting autonomous behaviors were surprisingly robust. During tracking, we observed remarkable recovery from occlusion and objects leaving the robot’s field of view.

During fully autonomous untethered operation, we achieved long term deployments in environments containing challenging visual features such as reflections in the NEA Giant Ocean Tank and variable artificial lighting throughout the exhibit.

Taken together, these results on challenging, real-world tasks in complex environments establish a baseline and open up several promising directions for further improvement. On the perception side, our full track-anything pipeline currently exceeds the compute budget of the low-cost Raspberry Pi onboard the robot, which creates a clear opportunity: either migrate to a more capable edge platform (e.g., an NVIDIA Jetson) or further refine our lightweight embedded tracker so that it approaches the performance of the heavier pipeline. On the hardware and control side, co-optimizing flipper morphology and gait parameters offers a natural path to faster, more efficient swimming, enabling longer-range missions and more reliable tracking. For extended autonomous deployments, navigation is another lever: whereas most conventional AUVs rely on Doppler Velocity Loggers (DVLs) for dead reckoning, we plan to explore integrating compact DVLs [43] alongside more experimental long-range navigation strategies tailored to biomimetic AUVs [44]. Finally, while the policies described here already exhibit robust tracking and obstacle avoidance, more structured recovery behaviors—both for re-acquiring lost targets and for disentangling from complex environments could further enhance reliability and mission duration. These next steps will result in increasingly capable and resilient bio-inspired AUVs for real-world marine monitoring and field operations.

Finally, recent studies have suggested that biomimetic robots can reduce response in wild animals, and that turtle-like forms in particular reduce flee responses in many organisms [12, 31]. In our experiments, qualitatively, the animals tracked in the aquarium had no noticeable change in behavior with the introduction of Crush, other than one of the turtles approaching and biting the yellow tether in early experiments. However, further studies are needed to understand animal-robot interactions in the wild

and to validate the potential value (or lack thereof) of using biomimetic robots for marine observational science.

4 Methods

4.1 Fabrication and Hardware

Crush houses all its electronics in a 100 mm inner diameter, 300 mm long Blue Robotics Watertight enclosure tube, made from cast acrylic plastic and rated to depths up to 1000 m in salt water. Its onboard electronics include a Raspberry Pi 5, motor controllers, a pressure sensor, 9 axis IMU, and various components for communication, power management, and heat dissipation. For vision, we embed two exploreHD 3.0 (400 meter depth) Underwater ROV/AUV USB General Vision Cameras into the turtle head of the robot. The flippers are injection molded using a custom molding setup. Each flipper consists of a loosely bioinspired 3D printed "skeleton", which constrains the motion of the proximal flipper, and a silicone matrix that is overmolded (in a similar procedure to [45–47]) onto the skeleton to provide flexible hydrofoil dynamics, which have been shown to result in more effective locomotion. The flippers are attached to 3DOF shoulders consisting of Dynamixel XW540-T260-R motors. While these motors are officially rated for low depth operation in fresh water (1 meter for 24 hours), we found that deployment in saltwater was not possible without further modification. The weak point for water entry into the motors is the connector from the wire to the motor housing. To insulate this connection from saltwater, we used marine epoxy to cover the connector-to-motor interface. After this modification, the motors were able to reliably function for hour-long deployments at about 10 meter depths. The turtle’s head, chassis, and shell were all printed from ABS on a Bambu P1S with 100% infill to prevent absorption of water into these components.

4.2 Biomimetic locomotion

Crush’s locomotion policy is based on trajectories derived from the motion capture analysis of green sea turtles that were originally characterized by Van der Geest et.al [39]. The Van der Geest trajectories are sinusoidal functions that specify a straight swimming gait for 3DOF shoulder joints, and can be directly used to produce forward locomotion for our robot. Because these trajectories are time-parametrized, we can alter the speed by adjusting the frequency. To achieve pitch control, yaw control, and roll control, we apply a series of transformations to the base gait. First, for pitch control, we systematically offset the final joint of the flippers, which has the effect of altering the angle of attack of the flipper, changing the direction of the resulting thrust vector. For yaw control, we simply reduce the amplitude of the limb movement in the direction of the turn, resulting in a net torque that reorients the body. For roll control, we apply similar transformations as for pitch control, but we rotate the hydrofoils in opposite directions, causing a roll component of torque to emerge. Finally, we also hand designed a backwards gait to allow the turtle to swim (more slowly) in reverse.

These gaits are operationalized as follows. First, we construct a vector of control inputs,

$$\mathbf{u} = [u_{\text{freq}}, u_{\text{roll}}, u_{\text{pitch}}, u_{\text{yaw}}]^T, \quad (1)$$

where u_{fwd} governs the locomotion frequency and the other elements correspond to desired rotations in 3D space. Each element of is a scalar value such that $\mathbf{u}_i \in [-1, 1]$. Thus, for example for pitch, we have a maximum pitching angle, θ_{max} of the hydrofoils (arbitrarily set based on parametrization). The control input u_{pitch} then applies the following transformation to the distal joint that controls the inclination of the hydrofoil:

$$\mathbf{q}_{\text{des,pitch}} = \mathbf{q}_{0,\text{pitch}} + \theta_{\text{max}} u_{\text{pitch}}, \quad (2)$$

where $\mathbf{q}_{0,\text{pitch}}$ is the baseline gait from the Van der Geest trajectories. Yaw control behaves similarly, but rather than applying an offset, the control input simply applies a decimal fraction of the baseline amplitude to apply yaw:

$$\mathbf{q}_{\text{des}} = \mathbf{q}_0 * (u_{\text{pitch}} + 1.0). \quad (3)$$

Finally, roll control applies the same transformation as pitch, but with a different threshold θ_{max} . We implement these trajectories via a joint-space trajectory tracking controller [48] defined as follows:

$$\tau(t) = \mathbf{K}_p(\mathbf{q}_{\text{des}}(t) - \mathbf{q}(t)) + \mathbf{K}_d(\dot{\mathbf{q}}_{\text{des}}(t) - \dot{\mathbf{q}}(t)), \quad (4)$$

where $\mathbf{u}(t) \in \mathbb{R}^6$ is the control signal (joint velocities), $\mathbf{q}_{\text{des}}(t)$ and $\dot{\mathbf{q}}_{\text{des}}(t)$ are the desired joint positions and velocities from biological motion primitives, $\mathbf{q}(t)$ are measured joint positions, and \mathbf{K}_p is a diagonal proportional gain matrix, which we tune for our specific platform.

To augment the robot’s performance, we take inspiration from real sea turtles and use the rear flippers as rudders to aid in pitch control and stabilization. The pitch of the rear flippers effects the overall pitching of the robot. If the rear flippers are pitched down (up) the robot tends to pitch down (up). For pitch control, we take the desired pitch of the robot, scale that to the range of the rear flipper pitch joint, and use it as a setpoint for a PD controller. Active stabilization helps mitigate pitching oscillations of the head and thus the camera feed (active stabilization is made necessary by the lack of active neck). The active stabilization routine is implemented as a sinusoidal oscillation of the rear flippers at the frequency of the front flipper gait. It is designed such that during the downstroke while the robot tends to pitch up the rear flippers pitch down to counter that pitching motion. The same logic in reverse applies during the upstroke.

4.3 Track Anything

We implement a real-time, human-in-the-loop tracking pipeline composed of two phases: (1) interactive object initialization via point-prompted segmentation and (2) online mask propagation. Initialization is performed with the Segment Anything Model (SAM) [41] and propagation/tracking with the CUTIE tracker [42]. The system targets

low-latency operation on the live video streams (the turtle-mounted cameras), preserving continuous operator visibility and enabling on-demand corrective re-initialization for robust long-horizon tracking.

Real-time video acquisition and display. A dedicated capture (parallel) thread continuously reads frames from the live stream and maintains a single-element buffer (size = 1), discarding stale frames to minimize end-to-end latency. A rendering thread consumes the most recent frame and, (when available) overlays the current segmentation mask and centroid, providing operator situational awareness. This decoupled design ensures immediate access to the latest frame while avoiding backlog accumulation.

Initialization via SAM. To initialize (or re-initialize) a target, the operator provides a small set of point prompts on the currently displayed frame:

- **Positive prompts (left-clicks):** points placed inside the object of interest (label 1).
- **Negative prompts (right-clicks):** points placed outside the object (label 0).

Upon receiving $x = 3$ total prompts within $\Delta t \leq 3$ s (with at least one positive), the system invokes SAM on the *latest captured frame* and the labeled points. SAM returns a binary mask, which we compute its centroid; these serve as inputs to the tracker and as outputs to downstream consumers (the controller). Tying segmentation to the most recent frame avoids drift due to display lag and reduces operator effort for high-precision initialization.

Online mask propagation/tracking via CUTIE For each subsequent frame, the current binary mask and the next frame are passed to CUTIE tracker, which predicts the next-frame mask. From this prediction, we extract the centroid and stream both the mask and centroid to the downstream controller. The tracker runs continuously and independently of the display pipeline. Lightweight health signals (mask area change, centroid displacement, and tracker confidence) are computed to detect anomalies; large deviations trigger a *soft-alert* (visual indicator) but do not interrupt tracking.

On-demand corrective re-initialization (human-in-the-loop). A correction listener thread runs in parallel and monitors for a *two-right-click* gesture occurring within a short window (≤ 2 s). This gesture indicates that the current mask is degraded or that a new target should be acquired. Once this occur:

1. The tracker, capture thread, and rendering thread, *continue running* to maintain temporal continuity and to still be up-to-date.
2. The system UI switches to an “init-pending” state, prompting the operator for three point prompts as above.
3. Once three prompts are received within $\Delta t \leq 3$ s, SAM is re-invoked on the most recent frame to produce a refreshed mask.
4. The tracker is warm-restarted using the new mask, and normal propagation resumes.

This protocol increases robustness in cluttered or dynamic scenes while avoiding hard interruptions to the controller.

Concurrency and state management. We formalize the system as a non-blocking state machine with four states:

- IDLE: video capture and rendering active; no active track.
- INIT: awaiting three prompts (≤ 3 s) to call SAM; on success, transition to TRACK; on timeout, revert to IDLE.
- TRACK: CUTIE propagates masks frame-by-frame; health signals computed; correction listener active; video capture and rendering active.
- CORRECT: two-right-click gesture detected; solicit three prompts; on success, re-initialize via SAM and return to TRACK.

Thread-safe queues connect capture, UI, segmentation, and tracking workers. Click debouncing prevents spurious gestures. All actions are logged with frame indices and timestamps for reproducibility.

The turtle follows the tracked object using the gaits described in Section 4.2 to perform visual servoing. To summarize, given a tracked object centroid position $[x, y]$ in a frame with width w and height h , the control inputs are modified based on the distance to the center of the frame as follows:

$$u_{\text{yaw}} = 2x/w - 1, \quad (5)$$

$$u_{\text{pitch}} = 2y/h - 1. \quad (6)$$

The centroid is then logged. If the track is lost, the robot attempts to recover by moving in the direction implied by the object from the last successful tracking frame. **Pool Experiments.** We chose a variety of objects for the robot to track, including a toy turtle, toy pig, human head and fish tail. We also had the robot track a swimmer who was free to swim around the pool. In total, we acquired around 45 minutes of tracking time in the pool, with minimal tracking errors.

4.4 Untethered Autonomy

4.4.1 Obstacle Avoidance

We rely on a small, USB-powered WiFi router to communicate with robot when in tetherless mode. However, once the robot is submerged in water, we have no way of communicating or interfering with its operation. Crush is equipped with its two forward-facing stereo cameras which are 54mm apart and record 640×480 pixel images at 30Hz. All image processing and navigation computations are performed onboard the Raspberry Pi 5 within the watertight enclosure of the robot. Stereo camera calibration was performed using the fisheye camera model in OpenCV [49]. Intrinsic parameters (camera matrices) and distortion coefficients, and extrinsic parameters (rotation matrix, etc.) were determined through checkboard calibration underwater, then validated in pool tests. Depth estimation from stereo cameras is done through the following pipeline. Firstly, due to computational limitations of the Raspberry Pi 5, this was executed at around 10Hz. Raw left and right images are undistorted and rectified using precomputed mapping functions, transforming them into aligned grayscale images suitable enough for correspondence matching. Then, we perform stereo block

matching using the StereoBM algorithm, which computes the disparity map representing the horizontal pixel displacement between corresponding points in the left and right images. Key parameters such as block size, number of disparities, and texture threshold were tuned empirically to balance accuracy and computation efficiency for underwater tetherless deployment. The raw disparity map undergoes filtering to smooth depth discontinuities and suppress invalid disparities. The filtered disparity map is then converted to a metric depth using the re-projection matrix, \mathbf{Q} , previously obtained from stereo calibration using the following equation:

$$z(u, v) = \frac{Q_{2,3}}{Q_{3,2} \cdot d(u, v)} \quad (7)$$

where $z(u, v)$ is the depth in meters at pixel coordinates (u, v) , and \mathbf{Q} encodes the stereo geometry. Infinite depth values (from zero disparity) are replaced with the median finite depth within the region of interest. Pixels with a depth less than 3.0 meters are classified as obstacles and segmented using binary thresholding. We use OpenCV’s contour detection method to identify contours exceeding 3% of the field of view, as well as the corresponding centroids. We apply temporal filtering every 15 frames to reduce the influence of false detections. During an obstacle encounter, the control inputs are adjusted to steer the robot away from the obstacle while maintaining desired depth. Leveraging the gait control described in Section 4.2 when encountering an obstacle, the robot is commanded to produce maximum yaw ($u_{\text{pitch}} = \pm 1$) opposite of the direction of the centroid of the main contour, while also commanding a maximum roll ($u_{\text{roll}} = \pm 1$) to "bank" along the obstacle to increase agility of the turn. The robot executes the maneuver until the filtered stereo depth reading has risen past the threshold.

Acknowledgements. We would like to thank the New England Aquarium for allowing us to conduct experiments in their Great Ocean Tank, and we would like to thank the MIT DAPER for use of their swimming pool for experiments.

Declarations

- Funding: SMART M3 program, GIST Physical AI, BARI
- Conflict of interest: N/A
- Ethics approval: The experimental protocol at the New England Aquarium was approved by an IACUC.
- Data availability: Data is available at <https://github.com/zpatty/drl-turtle>
- Materials availability: N/A
- Code availability: Code is available at <https://github.com/zpatty/drl-turtle>
- Contributions: DR contributed to conceptualization, idea formation and aims, analysis, methodology, experimentation and validation, writing, and funding; ZJP contributed to conception, design, software, experiments, and writing. ES contributed to design, software, experiments, and writing. LC contributed to experiments and writing. DK contributed to experiments and writing. AM contributed to software and writing. PS contributed to experiments and writing.

References

- [1] Cardenas, J.A., Samadikhoshkho, Z., Rehman, A.U., Valle-Pérez, A.U., León, E.H.-P., Hauser, C.A., Feron, E.M., Ahmad, R.: A systematic review of robotic efficacy in coral reef monitoring techniques. *Marine pollution bulletin* **202**, 116273 (2024)
- [2] Besson, M., Alison, J., Bjerge, K., Goroehowski, T.E., Høyve, T.T., Jucker, T., Mann, H.M., Clements, C.F.: Towards the fully automated monitoring of ecological communities. *Ecology letters* **25**(12), 2753–2775 (2022)
- [3] Yoerger, D.R., Govindarajan, A.F., Howland, J.C., Llopiz, J.K., Wiebe, P.H., Curran, M., Fujii, J., Gomez-Ibanez, D., Katija, K., Robison, B.H., *et al.*: A hybrid underwater robot for multidisciplinary investigation of the ocean twilight zone. *Science Robotics* **6**(55), 1901 (2021)
- [4] Liu, K., Ding, M., Pan, B., Yu, P., Lu, D., Chen, S., Zhang, S., Wang, G.: A maneuverable underwater vehicle for near-seabed observation. *Nature Communications* **15**(1), 10284 (2024)
- [5] Paull, L., Saeedi, S., Seto, M., Li, H.: Auv navigation and localization: A review. *IEEE Journal of oceanic engineering* **39**(1), 131–149 (2013)
- [6] Li, G., Wong, T.-W., Shih, B., Guo, C., Wang, L., Liu, J., Wang, T., Liu, X., Yan, J., Wu, B., *et al.*: Bioinspired soft robots for deep-sea exploration. *Nature Communications* **14**(1), 7097 (2023)
- [7] Li, G., Liu, G., Leng, D., Fang, X., Li, G., Wang, W.: Underwater undulating propulsion biomimetic robots: A review. *Biomimetics* **8**(3), 318 (2023)
- [8] Katzschmann, R.K., DelPreto, J., MacCurdy, R., Rus, D.: Exploration of underwater life with an acoustically controlled soft robotic fish. *Science robotics* **3**(16), 3449 (2018)
- [9] Baines, R., Patiballa, S.K., Booth, J., Ramirez, L., Sipple, T., Garcia, A., Fish, F., Kramer-Bottiglio, R.: Multi-environment robotic transitions through adaptive morphogenesis. *Nature* **610**(7931), 283–289 (2022)
- [10] Li, G., Chen, X., Zhou, F., Liang, Y., Xiao, Y., Cao, X., Zhang, Z., Zhang, M., Wu, B., Yin, S., *et al.*: Self-powered soft robot in the mariana trench. *Nature* **591**(7848), 66–71 (2021)
- [11] Prakash, A., Nair, A.R., Arunav, H., PR, R., Akhil, V., Tawk, C., Shankar, K.V.: Bioinspiration and biomimetics in marine robotics: a review on current applications and future trends. *Bioinspiration & Biomimetics* **19**(3), 031002 (2024)

- [12] Kruusmaa, M., Gkliva, R., Tuhtan, J., Tuvikene, A., Alfredsen, J.A.: Salmon behavioural response to robots in an aquaculture sea cage. *Royal Society open science* **7**(3), 191220 (2020)
- [13] Jessop, S.A., Saunders, B.J., Goetze, J.S., Barrett, N.S., Harvey, E.S.: A comparison of the behavioural responses of fishes to a remotely operated vehicle and diver-based stereo-video sampling. *Estuarine, Coastal and Shelf Science* **298**, 108621 (2024)
- [14] Cai, L., Jézéquel, Y., Mooney, T.A., Girdhar, Y.: Measuring and minimizing disturbance of marine animals to underwater vehicles. *arXiv preprint arXiv:2506.11335* (2025)
- [15] Ramirez-Llodra, E., Brandt, A., Danovaro, R., De Mol, L., Escobar, E., German, C.R., Levin, L.A., Martinez Arbizu, P., Menot, L., Buhl-Mortensen, P., *et al.*: Deep, diverse and definitely different: unique attributes of the world’s largest ecosystem. *Biogeosciences* **7**(9), 2851–2899 (2010)
- [16] Danovaro, R., Corinaldesi, C., Dell’Anno, A., Snelgrove, P.V.: An ecosystem-based deep-ocean strategy. *Science* **355**(6324), 452–454 (2017)
- [17] Hoegh-Guldberg, O., Bruno, J.F.: The impact of climate change on the world’s marine ecosystems. *Science* **328**(5985), 1523–1528 (2010)
- [18] Sala, E., Lubchenco, J., Grorud-Colvert, K., Novelli, C., Roberts, C., Sumaila, U.R.: Protecting the global ocean for biodiversity, food and climate. *Nature* **592**(7854), 397–402 (2021)
- [19] Fish, F.E., Lauder, G.V.: Passive and active flow control by swimming fishes and mammals. *Annual Review of Fluid Mechanics* **38**, 193–224 (2006)
- [20] Lauder, G.V., Tytell, E.D.: Hydrodynamics of undulatory propulsion. *Fish physiology* **23**, 425–468 (2005)
- [21] Sfakiotakis, M., Lane, D.M., Davies, J.B.C.: Review of fish swimming modes for aquatic locomotion. *IEEE journal of oceanic engineering* **24**(2), 237–252 (1999)
- [22] Zhai, Y., Tolley, M.T.: Electronics-free 3d-printed soft swimming robot with pneumatic oscillating control for efficient undulating locomotion. *IEEE Robotics and Automation Letters* (2025)
- [23] Triantafyllou, M.S., Triantafyllou, G.S.: An efficient swimming machine. *Scientific American* **272**(3), 64–70 (1995)
- [24] Lauder, G.V.: Fish locomotion: recent advances and new directions. *Annual Review of Marine Science* **7**, 521–545 (2015)
- [25] Fossen, T.I.: *Handbook of Marine Craft Hydrodynamics and Motion Control*.

John Wiley & Sons, Hoboken (2011)

- [26] Yuh, J.: Design and control of autonomous underwater robots: A survey. *Autonomous Robots* **8**(1), 7–24 (2000)
- [27] Girdhar, Y., McGuire, N., Cai, L., Jamieson, S., McCammon, S., Claus, B., Soucie, J.E.S., Todd, J.E., Mooney, T.A.: Curee: A curious underwater robot for ecosystem exploration. arXiv preprint arXiv:2303.03943 (2023)
- [28] Wyneken, J.: Sea turtle locomotion: mechanisms, behavior, and energetics. *The biology of sea turtles* **1**, 165–198 (1997)
- [29] Renous, S., Rimblot-Baly, F., Fretey, J., Bels, V.: Locomotion patterns in newer aquatic reptiles: A review of comparative locomotion and swimming patterns in marine turtles. *Journal of Experimental Biology* **211**(2), 274–289 (2008)
- [30] Krause, J., Ruxton, G.D., Krause, S.: Swarm intelligence in animals and humans. *Trends in ecology & evolution* **26**(1), 28–34 (2011)
- [31] Asunsolo-Rivera, A., Lester, E., Langlois, T., Vaughan, B., McCormick, M., Simpson, S., Meekan, M.: Behaviour of mesopredatory coral reef fishes in response to threats from sharks and humans. *Scientific Reports* **13**(1), 6714 (2023)
- [32] Chen, D., Wu, Z., Zhang, P., Tan, M., Yu, J.: Performance improvement of a high-speed swimming robot for fish-like leaping. *IEEE Robotics and Automation Letters* **7**(2), 1936–1943 (2022)
- [33] van der Geest, N., Garcia, L.: Employing Robotics for the Biomechanical Validation of a Prosthetic Flipper for Sea Turtles as a Substitute for Animal Clinical Trials. *Biomechanics* **3**(3), 401–414 (2023) <https://doi.org/10.3390/biomechanics3030033>
- [34] Wang, R., Wang, S., Wang, Y., Cheng, L., Tan, M.: Development and motion control of biomimetic underwater robots: A survey. *IEEE Transactions on Systems, Man, and Cybernetics: Systems* **52**(2), 833–844 (2020)
- [35] Licht, S., Hover, F., Triantafyllou, M.S.: Design of a flapping foil underwater vehicle. In: *Proceedings of the 2004 International Symposium on Underwater Technology* (IEEE Cat. No. 04EX869), pp. 311–316 (2004). IEEE
- [36] Salazar, J., Cai, L., Cook, B., Rus, D.: Multi-robot visual control of autonomous soft robotic fish. In: *2022 IEEE/OES Autonomous Underwater Vehicles Symposium (AUV)*, pp. 1–6 (2022). IEEE
- [37] Berlinger, F., Gauci, M., Nagpal, R.: Implicit coordination for 3d underwater collective behaviors in a fish-inspired robot swarm. *Science Robotics* **6**(50), 8668 (2021)

- [38] Wyneken, J.: The anatomy of sea turtles (2001)
- [39] van der Geest, N., Garcia, L., Nates, R., Godoy, D.A.: New insight into the swimming kinematics of wild Green sea turtles (*Chelonia mydas*). *Scientific Reports* **12**(1), 18151 (2022) <https://doi.org/10.1038/s41598-022-21459-y>
- [40] Lab, R.N.: Hawksbill sea turtle shell. Sketchfab 3D scan (2021). <https://sketchfab.com/3d-models/hawksbill-sea-turtle-shell-f94086eb89ca4160adae61a7140f7d27>
- [41] Kirillov, A., Mintun, E., Ravi, N., Mao, H., Rolland, C., Gustafson, L., Xiao, T., Whitehead, S., Berg, A.C., Lo, W.-Y., Dollar, P., Girshick, R.: Segment anything. In: *Proceedings of the IEEE/CVF International Conference on Computer Vision (ICCV)*, pp. 4015–4026 (2023)
- [42] Cheng, H.K., Oh, S.W., Price, B., Lee, J.-Y., Schwing, A.: Putting the object back into video object segmentation. In: *Proceedings of the IEEE/CVF Conference on Computer Vision and Pattern Recognition (CVPR)*, pp. 3151–3161 (2024)
- [43] Hasan, K., Ahmad, S., Liaf, A.F., Karimi, M., Ahmed, T., Shawon, M.A., Mekhilef, S.: Oceanic challenges to technological solutions: A review of autonomous underwater vehicle path technologies in biomimicry, control, navigation, and sensing. *IEEE Access* **12**, 46202–46231 (2024)
- [44] Gill, J.P., Taylor, B.K.: Navigation by magnetic signatures in a realistic model of earth’s magnetic field. *Bioinspiration & Biomimetics* **19**(3), 036006 (2024)
- [45] Patterson, Z.J., Sologuren, E.R., Rus, D.: Design of trimmed helicoid soft-rigid hybrid robots. In: *2025 IEEE 8th International Conference on Soft Robotics (RoboSoft)*, pp. 1–7 (2025). IEEE
- [46] Desatnik, R., Patterson, Z.J., Gorzelak, P., Zamora, S., LeDuc, P., Majidi, C.: Soft robotics informs how an early echinoderm moved. *Proceedings of the National Academy of Sciences* **120**(46), 2306580120 (2023) <https://doi.org/10.1073/pnas.2306580120>
- [47] Bell, M.A., Becker, K.P., Wood, R.J.: Injection Molding of Soft Robots. *Advanced Materials Technologies* **7**(1), 2100605 (2022) <https://doi.org/10.1002/admt.202100605>
- [48] Lynch, K.M., Park, F.C.: *Modern Robotics*. Cambridge University Press, Cambridge (2017)
- [49] Bradski, G.: The OpenCV Library. *Dr. Dobb’s Journal of Software Tools* (2000)
- [50] Tomasi, C., Kanade, T.: Detection and tracking of point. *Int J Comput Vis* **9**(137-154), 3 (1991)

Supplementary Information

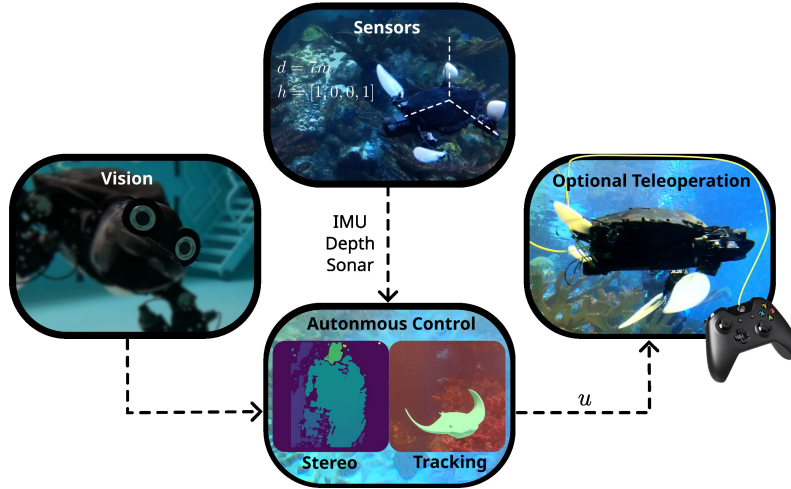


Fig. S1 System Diagram of Crush's Autonomous Control and Tasking: the robot is equipped with cameras and several sensors, allowing it to operate autonomously with manual override and high-level tasking capability.

S1 Turtle Characterization

Characterization was performed on the robot's maximum forward swimming speed, straight-line diving speed, and yaw rate. All characterization was performed in a swimming pool with small flow disturbances. Robot motion was tracked by external cameras in all cases; for forwards swimming and yaw rotation experiments, a camera mounted pool-side captured a sideways profile of the robot. For diving experiments, an underwater GoPro mounted near the bottom of the pool captured the entire dive trajectory of the robot from surface to pool floor. For forward swimming and diving experiments, the robot position was tracked in terms of pixels in the camera frame from start to finish of the trajectory. Tracking was semi-supervised; for each trajectory, we selected a keypoint on the turtle in the first frame, and then a MATLAB script applied the Kanade-Lucas-Tomasi (KLT) tracking algorithm [50] to track this keypoint on the robot across frames. Pixel distances were converted to robot body lengths by measuring the length of the robot in pixel space. For yaw rotation experiments, we counted the number of frames in between each full rotation of the robot and converted this to a yaw rate. Each characterization experiment was performed five times, and the results are reported in Fig. S2 as the average across the five experiments.

We found that the robot swims with a maximum forward speed of 0.32 BL/s (0.208 m/s) and a maximum yaw rate of 30 deg/s. The robot dives with a maximum speed of 0.18 BL/s. The calculated cost-of-transport ends up being 1.173.

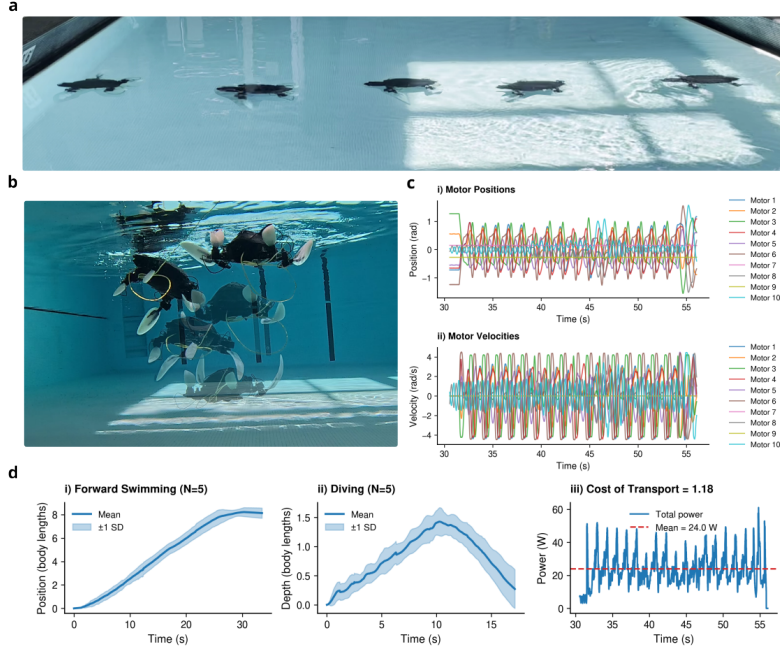


Fig. S2 Robotic Sea Turtle Characterization: **a)** Image sequence showing the robot’s forward swimming trajectory in a pool environment. **b)** Underwater view of the robot during a diving maneuver, demonstrating flipper-based propulsion and pitch control. **c)** Motor kinematics during steady swimming: **i)** joint positions showing synchronized oscillatory flipper motion across all 10 motors (front and rear flippers), and **ii)** corresponding motor velocities demonstrating consistent stroke patterns. **d)** Performance characterization across $N=5$ trials: **i)** Forward swimming speed showing mean position ± 1 standard deviation over 30 seconds, **ii)** diving behavior showing depth excursion of approximately 1.5 body lengths with controlled ascent and descent phases, and **iii)** power consumption profile during steady swimming with mean power of 24.0 W yielding a cost of transport of 1.18 (dimensionless). The robot demonstrates repeatable locomotion with low trial-to-trial variability in both forward swimming and diving maneuvers.

S2 CUTIE Tracker Failures

While the CUTIE tracker was remarkably robust even in the challenging aquarium environment, we observed the following failure modes in our experiments: (i) *Specular/mirror-induced duplicates (appearance duplication)*. When a target is adjacent to a mirror-like surface e.g., glass panels, the specular image is visually coherent with the real object and moves in a highly correlated manner. In close proximity, the displacement between the object and its reflection is small (even connected at the image space), so the appearance model and motion prior often conflate the two, producing early data-association errors (ID switches) or even mask mixing to one. As the object–reflection separation grows, tracks may fragment or bifurcate (the tracker “believes” one object split into two), causing confusion in the future step to track the wrong part or even a new object due to the learned behavior. (ii) *Low-light/low-contrast regimes (confidence collapse)*. When the tracked object enters a

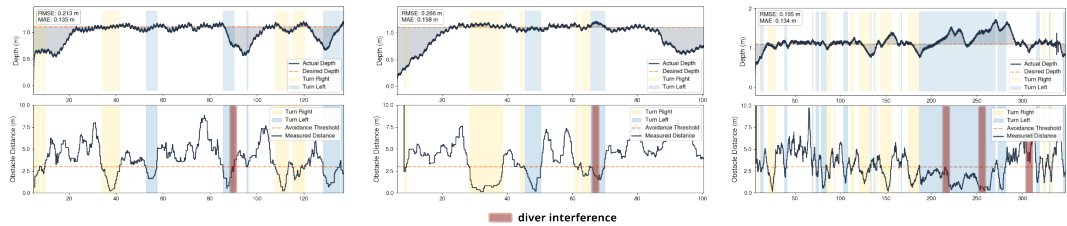


Fig. S3 Three untethered obstacle avoidance trials at the New England Aquarium (132 s, 94 s, and 341 s; left to right). For each trial, depth over time (top) and estimated obstacle distance (bottom) are shown, with yellow and blue shaded regions indicating right and left turn commands, respectively, and red shaded regions marking diver interference events. The robot maintained a 1.1 m target depth across all trials (RMSE = 0.213, 0.266, and 0.195 m; MAE = 0.135, 0.158, and 0.134 m) while executing 10, 7, and 28 avoidance maneuvers per trial, respectively. Across all three trials, the robot autonomously avoided 41 of 45 detected obstacles (91.1% success rate, 113.5 s per intervention), with the three wall-collision failures attributable to the glass tank environment rather than reef-relevant obstacles.



Fig. S4 Untethered toy turtle tracking over a 32-second window of a 3 min 34 s trial. Top row: external observer view of the robot pursuing the toy turtle. Bottom row: onboard stereo camera view with the FOMO-detected centroid (red dot) used by the motion planner to drive the robot's motor commands in real time.

dark, low-contrast and/or far zones, per-pixel tracking likelihoods from the tracker model become noise-dominated as the object is not clearly visible. Confidence over the target mask dropped below the gating threshold, suppressing detections and triggering track termination, even if the object is still in frame. (iii) *Stitching Line Distortions*. Since we stitch both camera views into one image. Fast motion that crosses or runs along the stitching seam exposes minor view or timing differences, producing seam-level splits or local distortions that break appearance/motion continuity and trigger fragmented tracks.

S3 Untethered Tracking

To enable untethered tracking, we implemented FOMO (Faster Objects, More Objects), trained in Edge Impulse Studio and optimized for real-time inference on the robot's Raspberry Pi 5 computer. FOMO is a centroid-based architecture designed for resource-constrained embedded platforms.

The training data for the FOMO models comprised several toy turtle images captured in both the SeaGrant tank and Alumni Pool settings at various distances and



Fig. S5 Tetherless Tracking Trials. Top-down view of the autonomous tracking robot pursuing a toy turtle target across multiple trials in the MIT Sea Grant testing tank. Each semi-transparent silhouette represents the robot at successive positions during left, right, and center target trials. The glass wall at the center of the tank presented detection challenges, requiring the target to be repositioned closer to the robot for reliable model detection.

orientations. We collected a total of 2760 images using a 75/25 train-test split. Images from the robot’s left and right stereo cameras were stitched together, and instances of the toy turtle were manually labeled. The training set also included images with no toy turtle present to improve robustness.

The trained model was deployed following the same procedure as the obstacle avoidance experiments, where a WiFi router was used to initialize the robot before submersion. The model was compressed to a float32 binary file format and integrated into the perception pipeline. Incoming images from the stereo cameras were passed through the model, which output a centroid location (or null if no turtle was detected) that was then passed to the robot’s motion planner.

We validated this model through a series of tracking trials targeting left-most, right-most, and center positions in the MIT SeaGrant testing tank (Fig. S5). Testing was conducted in a tank measuring $3.95\text{ m} \times 2.95\text{ m} \times 1.09\text{ m}$. The mean time to reach the toy turtle from one end of the tank to the other for left and right targets was 15.83 and 15.85 seconds, respectively. For trials where the target was placed at the center of the tank, however, the mean track time was 20.91 seconds, for the center of the tank was a glass wall, which proved difficult for the robot’s trained model to consistently detect. In fact, it required moving the target slightly closer to the robot in order for the model to detect the toy turtle.

Table S1 Analyses of pool and aquarium tracks

Animal Type	Track duration (secs)	Failed	End Track Reason
Turtle	59	No	stopped swimming
Turtle	57	No	stopped swimming
Turtle	43	No	visibility
Turtle	38	No	coral collision ^b
Turtle	36	No	depth limitation and visibility
Turtle	29	No	depth limitation
Turtle	23	Yes	tracker failure
Turtle	22	No	coral collision ^b
Turtle	20	Yes	user error
Turtle	12	No	swam into robot ^a
Turtle	9	No	depth limitation
Turtle	8	No	depth limitation
Stingray	32	No	swam over robot
Stingray	30	No	too fast
Stingray	22	Yes	tracker failure
Stingray	15	No	swam behind robot
Stingray	14	Yes	tracker failure
Stingray	13	No	swam under
Barricuda	20	No	depth limitation
Barricuda	15	Yes	tracker failure
Diver	45	No	NA
Diver	29	No	NA
Toy Turtle	249	No	NA
Toy Turtle	245	No	NA
Toy Turtle	223	No	NA
Toy Turtle	169	No	NA
Toy Turtle	161	No	NA
Toy Turtle	116	No	NA
Toy Turtle	96	No	NA
Toy Turtle	96	No	NA
Toy Turtle	83	No	NA
Toy Turtle	79	No	NA
Toy Turtle	71	No	NA
Toy Turtle	70	No	NA
Toy Turtle	57	No	NA
Toy Turtle	50	No	NA
Toy Turtle	47	No	NA
Toy Turtle	45	No	NA
Toy Turtle	36	No	NA
Toy Turtle	28	No	NA
Toy Turtle	23	No	NA
Toy Turtle	22	No	NA
Toy Turtle	20	No	NA
Toy Pig	133	No	NA
Toy Pig	67	No	NA
Toy Pig	21	No	NA
Fish Tail	106	No	NA
Human	93	No	NA
Human	79	No	NA
Human	65	No	NA
Human	31	No	NA
Plastic Head	92	No	NA

Several aquatic animals were observed and tracked in the Giant Ocean tank, as well as various objects in the swimming pool.

^a some tracks preemptively end early for the safety of the aquarium animals

^b track was not lost but ended early to prevent damage to robot